(life) of all such future vehicles will be experienced as 12.28 min using these engines. These results imply that 50% of all future landings will have descent times in excess of 12.28 min, but there is a real risk that there may not be enough time to cover the required minimum time of 6 required minutes in some landing attempts.

More precise risk information can be obtained using the reliability expressions. Application of the formulas in Table 2 results in a reliability of 0.7964 (BFE) and 0.5730 (BSE) using exponential PDF and 0.923 (BFE) and 0.8110 (BSE) using uniform PDF. These values are not very comforting, and the engines should be made stronger to last longer. A mean engine life of 30 min increases the reliabilities to 0.8913 (BFE) and 0.7436 (BSE) using exponential PDF and 0.9639 (BFE) and 0.9054 (BSE) using uniform PDFs. When the same order is used, a mean life of 60 min results in reliabilities of 0.9671, 0.9133, 0.9905, and 0.9733 for the same descent duration of 6 min. If 0.999 reliability is required, $R(t)$ expressions must be solved to find the parameters of the parent engine PDFs. The resulting mean values are as follows: 388.5 (BFE) and 666.7 (BSE) for exponential PDF and 188 (BFE) and 320 (BSE) for uniform PDF. This example illustrates the well-known diminishing returns in reliability calculations. Large improvements in each engine results in very small marginal gains in the overall system reliability. For example, the BSE system's engines (exponential case) would have to improve by a factor of 11 to increase system reliability by 9%.

Conclusions

This Note has addressed a new reliability configuration problem that may be needed in large future powered vehicle descent and possibly ascent design processes. Whereas Eqs. (3) and (5) are general for any parent PDF, it is not easy to derive closed-form reliability expressions for certain PDFs such as the normal and the general gamma distributions. Then, Monte Carlo simulation can be used in such cases. The specific formulas presented, however, can be used if exponential and uniform distributions are good representations for engine lives in a given problem. An analytical solution is always preferable over experimental (simulation) ones because the formulas are general for any given parameter. Another realistic extension should consider what happens to the life of the remaining engines as redundant pair fails. (Again, one engine of the pair fails and the opposite engine shut off.) The failure rates of the survivors must increase and simulation study may be appropriate. It is also assumed that all engines, within the pair and the entire vehicle, are independent of each other. This assumption may not always be true and the issue of dependency is a formidable mathematical challenge. This work would have to involve bivariate PDFs (instead of the univariate PDFs used in this Note) and/or correlation matrices to express statistical dependency among the engines within and across the engine pairs. The reader can refer to Johnson and Kotz[5] for an excellent discussion on multivariate (joint) PDFs with an emphasis on bivariate exponential PDF. Monte Carlo simulation will be necessary at some stage because analytical work quickly becomes highly intractable or impossible (even numerically) in dealing with dependent random variables found in engineering design problems.

References

[1]Brown, N., Hirata, C., and Shannon, R., "Mars Scheme: The Mars Society of Caltech Human Exploration of Mars Endeavor," *Third International Mars Society Convention*, Paper No. 5 in Track 2A, Aug. 2000.

[2]Brown, N., and Hirata, C., "The Mars Scheme IV: Trajectory Analysis," *Fourth International Mars Society Convention*, Paper No. 3 in Track 2D, Aug. 2001.

[3]Lewis, E. E., *Introduction to Reliability Engineering*, 2nd Ed., Wiley, New York, 1996.

[4]Sarper, H., "Extreme Value Flight Duration Analysis of Four Engine Spacecraft," *Journal of Spacecraft and Rockets*, Vol. 34, No. 3, 1997, pp. 402–405.

[5]Johnson, N. L., and Kotz, S., *Distributions in Statistics: Continuous Multivariate Distributions*, Wiley, New York, 1972, Chap. 4.

J. A. Martin
Associate Editor

Computational Investigation of Three-Dimensional Flow Effects on Micronozzles

R. D. D. Menzies,* B. E. Richards,† K. J. Badcock,‡
J. Löseken,§ and M. Kahl§
*University of Glasgow,
Glasgow, Scotland G12 8QQ, United Kingdom*

Introduction

SINCE the launch of Sputnik in 1957, there has been a steady growth in the size and weight of satellites. However, advances in miniaturization provide an opportunity to use smaller satellites. Microspacecraft development is technically demanding. Miniaturization is required in every subsystem including propulsion. Microelectromechanical systems (MEMS) is a new technology that can aid in the miniaturization of the propulsion system.

Deep reactive ion etching (DRIE) is one method among others of producing MEMS nozzles and is inherently two-dimensional. A material is placed on a two-dimensional silicon wafer, and a chemical reaction causes the nozzle pattern to be etched through to the wafer. Glass sheets are then anodically bonded to close the open channel. The silicon wafers used in recent experiments[1,2] were 308 μ thick, giving a nozzle depth H of 308 μ and a throat width typically of between 19 and 38 μ. A typical exit diameter is 100 μ, twice the size of a human hair.

Nearly all spacecraft nozzle shapes have been designed using inviscid flow theory. However, when dealing with such small devices the Reynolds numbers are low giving large boundary layers. The problem of low-Reynolds-number micronozzle flows has been examined at Massachusetts Institute of Technology (MIT),[1,2] where contoured converging-diverging nozzles were created and mass flow rates and thrusts measured. As the models had a large depth in comparison to the throat width, a two-dimensional model was used to predict viscous nozzle flow allowing comparison between experimental and computational measurements. It was found that experimentally measured mass flow rates matched well with predictions, whereas there was considerable discrepancy in thrust. This effect was presumed to be caused by the growth of the boundary layers on the upper and lower nozzle surfaces.

The aim of this work is to verify the findings for two-dimensional computations and experiment and then to investigate the extent of the three-dimensional effects. The computations have been done using the University of Glasgow's flow solver, Parallel Multi-Block (PMB).[3] Solutions were considered fully converged when the maximum residual had dropped eight orders of magnitude. Grid convergence was tested by running the calculations with double and half the number of grid points in each direction compared to a standard grid. Solutions were near identical for all grids used and were considered fully grid independent.

*Research Student, Department of Aerospace Engineering, Computational Fluid Dynamics Group; rmenzies@aero.gla.ac.uk.

†Mechan Professor, Department of Aerospace Engineering, Computational Fluid Dynamics Group. Associate Fellow AIAA.

‡Senior Lecturer, Department of Aerospace Engineering, Computational Fluid Dynamics Group.

§Undergraduate Student, Department of Aerospace Engineering, Computational Fluid Dynamics Group.

Performance Measures and Boundary Conditions

We require a measure of the effectiveness of a nozzle to allow comparison. The main parameters of interest are the thrust F_t and specific impulse I_{sp} and how they change with variations in chamber pressure P_0 and Reynolds number Re. The Reynolds number is defined for conditions at the nozzle throat, using nozzle throat width for the length scale. F_t can be determined as

$$F_t = \dot{m}u_{exit} + (p_{exit} - p_\infty)A_{exit} \qquad (1)$$

Here, $\dot{m}$ is the mass flow rate, A is a reference area, and u is the x component of velocity. The specific impulse I_{sp} is defined as the thrust per weight flow. Other performance measures compare the performance to the ideal inviscid flow case. Thus, the coefficient of discharge is defined as the ratio of the viscous to inviscid predicted mass flow rates, and the thrust efficiency is given as the ratio of the viscous to inviscid predicted thrusts. Inviscid values can be determined from a solution of the Euler equations.

The boundary conditions that need to be defined in the problem can be seen in Fig. 1 for the three-dimensional case. The two-dimensional case is similar but does not have the top and bottom walls. The reservoir boundary condition is defined as follows: first, the u velocity is extrapolated from the interior of the domain, and v and w velocity components are set to zero. Second, entropy and enthalpy are given by the reservoir values. For the viscous cases an isothermal wall condition is assumed. The no-slip condition is imposed with zero normal pressure gradient.

Examination of Results

Comparison Between Experiment and Computation

In the experimental studies carried out at MIT by R. L. Bayt,[2] several geometries were studied. Comparisons between experiment and computation will only focus on expansion ratios of $\epsilon = 7.1$ and 5.4 for brevity.

Figure 2 shows a graph of the mass flow rates for $\epsilon = 7.1$. There is a good agreement between the measured and computed data. It is also clear that the differences between the two- and three-dimensional computations is small. The mass flow rate decreases as
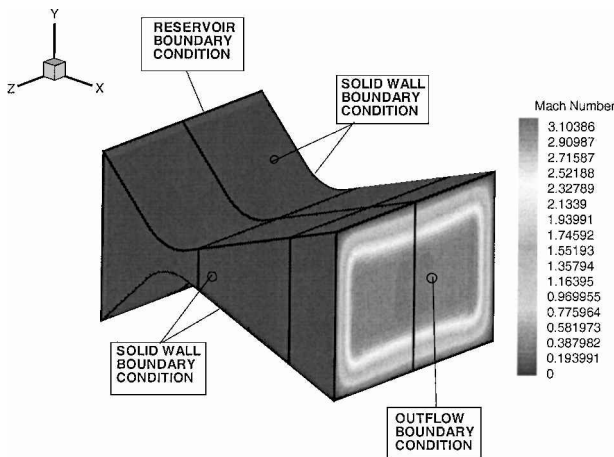

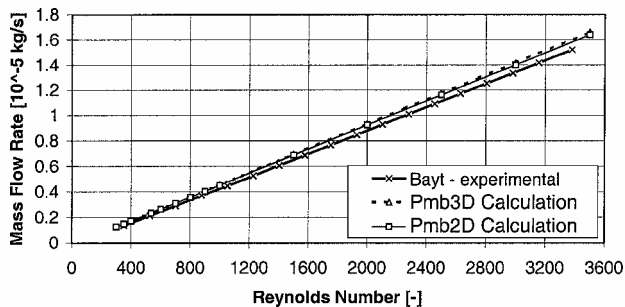Fig. 1   Nozzle boundary conditions for $\epsilon = 7.1$ showing contours of Mach number.

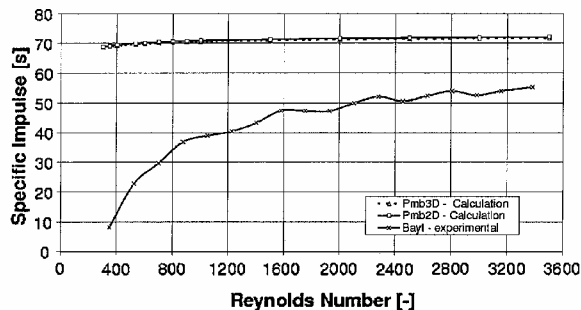Fig. 2   Comparison of measured and calculated mass flow rates: $\epsilon = 7.1$ and $D = 34$ μm.

Fig. 3   Comparison of measured and calculated specific impulse: $\epsilon = 7.1$ and $D = 34$ μm.
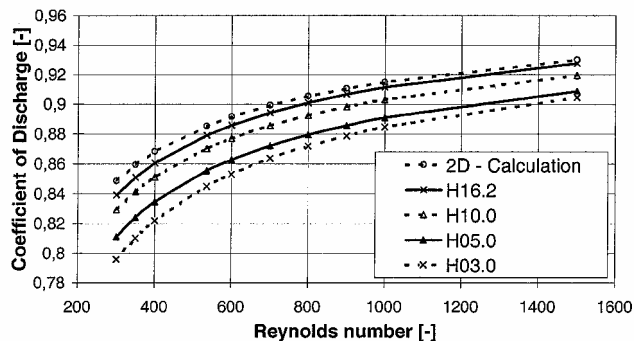

Fig. 4   Comparison of C_d vs Re for varying aspect ratios: $\epsilon = 5.4$.

the Reynolds number decreases because reduced Reynolds numbers can cause significant boundary-layer growth and blockage in the diverging section of the nozzle. Mach-number contours are plotted in Fig. 1 for a nozzle with an expansion ratio of 7.1 at a Reynolds number of 1000 and shows that the main boundary layer buildup is on the diverging section of the wall. The size of the boundary layer on the side walls is small in relation to the depth of the nozzle, and this explains the close agreement between two- and three-dimensional results.

The experimentally and computationally derived specific impulse is plotted in Fig. 3 for a range of Reynolds numbers. The computational values match well, but the divergence between the experimental and computational values is significant. This divergence is primarily because the specific impulse is a derived value and thus amplifies differences. It should also be remembered that the thrust stand used to measure the thrust in the experiments is accurate only to ± 0.2 mN. However, there is the added problem that the thrust plate offers no damping, and so, consequently, the accuracy reduces to ± 1 mN. Maximum thrusts are of the order of 15 mN, and so the possible error is significant. In summary, it can be said that the results for the mass flow rate are satisfactory. The two- and three-dimensional computations match very closely and are very similar to experiment. Agreement for the thrust is reasonable, given the uncertainty in the measurements.

Spontaneous condensation in hypersonic flow was considered as a possible reason for the deviations for thrust. However, it was discovered that the gas used in the experiments was dry nitrogen (no water vapor should be present in the gas), and so this theory was eliminated.

Examination of the Extent of Three-Dimensional Viscous Effects

It has been shown that the extent of the three-dimensional viscous effects was smaller than previously thought for the nozzles just examined and that discrepancies between computations and experiments was caused by another source, possibly experimental errors. However the nozzles looked at earlier had large cross-sectional throat aspect ratios v. Nozzles with a constant expansion ratio of 5.4 and aspect ratios at the throat of 16.2, 10.0, 5.0, and 3.0 have been examined over a range of Reynolds numbers. Experimental tests were not performed for aspect ratios below around 8:1. Lower aspect ratios are plotted here to show the trend.
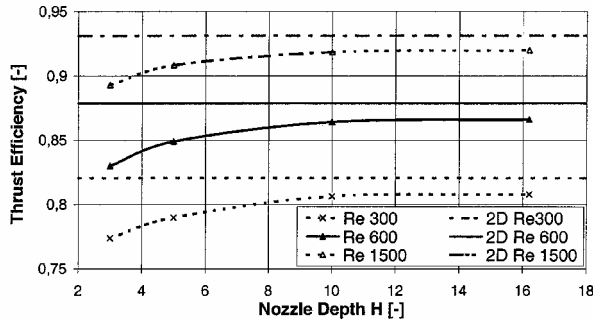
Fig. 5 Comparison of μ_{thrust} vs H for varying Re: $\epsilon = 5.4$.

Figure 4 shows the coefficient of discharge for these cases. The general trend is as expected, with an increase in throat aspect ratio leading to a solution that tends toward the two-dimensional solution as the viscous side-wall effects become less influential. Figure 5 shows a comparison between two- and three-dimensional results for throat aspect ratios and thrust efficiencies over specific Reynolds numbers. Increasing aspect ratio leads to a solution similar to that in two-dimensions. Throat aspect ratios below 10 appear to occur when three-dimensional effects are most prevalent.

Conclusions

This Note has examined the three-dimensional viscous effects in micronozzles by means of comparison with experimental data and two-dimensional computations. The main results can be summarized as follows: first, three-dimensional viscous effects are not the primary cause of divergence between two-dimensional predic-

tions and experimental data. For the nozzle geometries examined experimentally, the throat aspect ratio is large enough so that viscous side-wall effects have little influence. Second, an examination of varying throat aspect ratios shows that increasing the aspect ratio tends to produce results similar to the two-dimensional case. A similar trend was witnessed if the Reynolds number was increased as boundary-layer effects are reduced. It was found that below an aspect ratio of around 10 three-dimensional effects begin to become significant. Third, causes for the discrepancy in thrust were examined. Spontaneous condensation was ruled unlikely. Experimental measurements of this scale are very challenging, and it is probable that the error present in the experimental work is a contributing factor to the differences with this computational work.

Acknowledgment

The authors gratefully appreciate the help of Robert L. Bayt for permission to publish experimental data.

References

[1]Bayt, R. L., Ayon, A. A., and Breuer, K. S., "A Performance Evaluation of MEMS-Based Micronozzles," AIAA Paper 97-3169, July 1997.

[2]Bayt, R. L., "Analysis, Fabrication, and Testing of a MEMS-Based Micropropulsion System," Ph.D. Dissertation, Dept. of Aeronautics and Astronautics, Massachusetts Inst. of Technology, Cambridge, MA, June 1999.

[3]Badcock, K. J., Richards, B. E., and Woodgate, M. A., "Elements of Computational Fluid Dynamics on Block Structured Grids Using Implicit Flow Solvers," *Progress in Aerospace Sciences*, Vol. 36, 2000, pp. 351–392.

W. E. Williamson
Associate Editor

Errata

Payload Deployment by Reusable Launch Vehicle Using Tether

K. D. Kumar
National Aerospace Laboratory, Tokyo 181 0015, Japan

EQUATION (1) should be read as follows:

$$\ddot{R} = \dot{\theta}^2 R - \frac{\mu}{R^2} + \frac{3}{2}\frac{\mu}{R^2}\frac{M_e}{M}\frac{L^2}{R^2}(1 - 3\cos^2\beta\cos^2\eta)$$

$$\ddot{\theta} = -2\frac{\dot{R}}{R}\dot{\theta} + \frac{3}{2}\frac{\mu}{R^3}\frac{M_e}{M}\frac{L^2}{R^2}\sin 2\beta\cos^2\eta$$

$$\ddot{\beta} = 2\frac{\dot{R}}{R}\dot{\theta} - (\dot{\theta} + \dot{\beta})\left[(2 + \mu_c)\frac{\dot{L}}{L} - 2\dot{\eta}\tan\eta\right]$$

$$-\frac{3}{2}\frac{\mu}{R^3}\left(\sin 2\beta + \frac{M_e}{M}\frac{L^2}{R^2}\sin 2\beta\cos^2\eta\right)$$

$$\ddot{\eta} = -(2 + \mu_c)\frac{\dot{L}}{L}\dot{\eta} - \frac{1}{2}(\dot{\theta} + \dot{\beta})^2\sin 2\eta - \frac{3}{2}\frac{\mu}{R^3}\cos^2\beta\sin 2\eta$$

$$\ddot{L} = \left[(\dot{\theta} + \dot{\beta})^2\cos^2\eta + \dot{\eta}^2 - \frac{\mu}{R^3}(1 - 3\cos^2\beta\cos^2\eta)\right]L$$

$$+ \mu_c\frac{L}{2}\left[-\frac{\dot{L}^2}{L^2} + (\dot{\theta} + \dot{\beta})^2\cos^2\eta + \dot{\eta}^2\right.$$

$$\left. - \frac{\mu}{R^3}(1 - 3\cos^2\beta\cos^2\eta)\right] - \frac{\text{EA}}{M_e}\varepsilon_t U(\varepsilon_t)$$

$$- 2\zeta\left(\frac{\text{EA}}{M_e L_0}\right)^{\frac{1}{2}}(\dot{L} - \dot{L}_0) \tag{1}$$

where $\mu_c = (L/M_e)(dM_e/dL) = (1/M_e)(m_t/3M)[(m_2 + m_t/2) - 2(m_1 + m_t/2)]$.